Recent Advances in Polymer Network Liquid Crystal Spatial Light Modulators

Jie Sun, Shin-Tson Wu

CREOL, The College of Optics and Photonics, University of Central Florida, 4000 Central Florida Blvd, Orlando, Florida 32816
Correspondence to: S.-T. Wu (E-mail: swu@mail.ucf.edu)

Received 22 August 2013; revised 19 September 2013; accepted 20 September 2013; published online 00 Month 2013
DOI: 10.1002/polb.23391

ABSTRACT: Polymer network liquid crystal (PNLC) spatial light modulators are attractive for display and photonic applications because they can achieve submillisecond response time while keeping a large phase change. However, their on-state scattering caused by the grain boundary of LC multidomains hinders their applications. In this article, we review recent progress on the development of scattering-free PNLCs extending from short-wavelength infrared to visible region by reducing the domain sizes to ~200 nm through low temperature curing process. To reduce operation voltage, both transmissive and reflective modes, LC material properties (birefringence and dielectric anisotropy), polymer composition and concentration, and pretilt angle effect are analyzed. © 2013 Wiley Periodicals, Inc. J. Polym. Sci., Part B: Polym. Phys. **2013**, *00*, 000–000

KEYWORDS: fast switching; LCOS; light scattering; liquid-crystalline polymers (LCP); optics; polymer; spatial light modulator

INTRODUCTION Amplitude, phase, wavelength, and polarization are four major characteristics of a light wave. Liquid crystal (LC) spatial light modulator (SLM) is a useful electro-optic device for modulating the intensity, phase, and polarization state of an incident light because of its relatively low operation voltage, high birefringence, and broad bandwidth.[1] SLM has been widely used in display and photonic areas, such as digital hologram generation for three-dimensional display,[2–4] dynamic scanning films for time-multiplexed autostereoscopic display,[5] optical phased array for laser beam steering,[6] adaptive optics for wavefront correction,[7,8] and diffractive optical element for spectral filtering.[9] In most of these applications, fast response time and large phase modulation depth ($\geq 2\pi$) are required.

The response time of a nematic LC device is governed by several factors, such as cell gap, visco-elastic coefficient and applied voltage.[10] For a typical nematic LC device, the rise time can be greatly shortened by applying an overdrive voltage;[11] however, the decay time is still determined by the restoring elastic torque. This problem gets worse as the wavelength increases, for example, IR region, due to the need of a thicker cell gap for compensating the longer wavelength and lower birefringence.[12] A typical LC decay time for a 10-μm E7 LC cell (for 2π phase change) is ~200 ms. There is an urgent need to reduce the LC response time to submillisecond range while keeping a 2π phase change.

To improve the response time of a SLM, several approaches have been proposed. Dual frequency LC exhibits a positive dielectric anisotropy ($\Delta\varepsilon$) at low frequencies and negative $\Delta\varepsilon$ at high frequencies, so it can speed up both rise and decay times of a LC device by controlling the applied frequency.[13–15] But, it requires a complicated driving scheme. Moreover, operating at a high frequency would cause dielectric heating which would shift the crossover frequency and result in performance instability.[16] Polymer-stabilized blue phase LC exhibits optical isotropy and fast response time due to its self-assembled nanostructure.[17–19] It is quite promising for next-generation information display, but difficult to achieve 2π phase change because its phase dynamic range is only one third of a nematic LC. Surface-stabilized ferroelectric LC can achieve 10-μs response time.[20,21] But because of its bistability, it requires sophisticated optical configuration to generate continuous phase modulation.

In comparison to the abovementioned approaches, polymer network LC (PNLC) can achieve submillisecond response time while maintaining a large phase shift.[22–27] It can also generate continuous phase change with a relatively simple driving scheme. In contrast to polymer-dispersed LC (PDLC) which consists of LC droplets embedded in a polymer matrix,[9] PNLC can be used for phase modulation and has a large phase dynamic range because of the high LC concentration and surface alignment. The major issue which hinders the widespread application of PNLC as a phase-only modulator is the power-on light scattering caused by LC

Jie Sun is currently working towards her Ph.D. degree at the College of Optics and Photonics, University of Central Florida, Orlando, FL, USA. Her research interests include fast-response liquid crystals for display and photonic applications.

Shin-Tson Wu received the Ph.D. degree from University of Southern California. He is a Pegasus professor at College of Optics and Photonics, University of Central Florida. He is a recipient of SID Slottow-Owaki prize, OSA Joseph Fraunhofer award, SPIE G. G. Stokes award, and SID Jan Rajchman prize. He was the founding Editor-in-Chief of IEEE/OSA Journal of Display Technology. He is a Fellow of SID, IEEE, OSA, and SPIE. In 2013, he was inducted to the National Academy of Inventors.

multidomains. Although it has been reported that high polymer ratio (60–70%) can result in scattering-free holographic PDLC with nanoscale droplet sizes, the required operating voltage is relatively high (15–20 V/μm).[9]

In this review article, we describe the physical mechanisms for achieving submillisecond-response scattering-free PNLC SLMs from $\lambda = 1.55$ μm, 1.06 μm, to a visible wavelength. To reduce voltage, we analyze the effects of LC birefringence (Δn) and $\Delta\varepsilon$, and polymer concentration and diffusion rate, and pretilt angle in both transmissive and reflective modes.

Fabrication Procedure

PNLC (also known as anisotropic LC gel) has been studied extensively as an electrically tunable scattering device.[22,28–30] Although a scattering-free PNLC requires smaller domain sizes, the fabrication procedure is quite similar. LC host is first mixed with a small amount of photoreactive difunctional monomer and some photoinitiator. This photo-polymerizable precursor is then filled into a LC cell with homogeneous alignment. After that, a UV curing process is carried out to induce the polymer network crosslinking. A schematic illustration of the fabrication procedure of PNLC is shown in Figure 1.

Response Time

For a nematic device, the dynamic response of LC director reorientation can be described by Ericksen-Leslie equation.[31] By solving this equation under single elastic constant and small angle approximations, the rise time and free relaxation time of a homogeneous alignment cell can be expressed as follows:

$$\tau_{rise} = \frac{\tau_0}{(V/V_{th})^2 - 1} \tag{1}$$

$$\tau_{decay} = \frac{\gamma_1 d^2}{K_{11}\pi^2} \tag{2}$$

where τ_{decay} is the free relaxation time, V is the applied voltage, V_{th} is the threshold voltage, γ_1 is the rotational viscosity, K_{11} is the splay elastic constant, and d is the cell gap. Overdrive and undershoot method can be used to accelerate the rise time and decay time.[11] However, to improve the free relaxation time τ_0, a small visco-elastic coefficient (γ_1/K_{11}) LC material or thinner cell gap is required.

In a PNLC device, LC molecules are electrically switchable but with a faster response time and a higher operating voltage. Without considering light scattering, the operation mode of a PNLC device is quite similar to its nematic counterpart. Thus, eq 2 can be extended to PNLC devices. Therefore, the fast response time of PNLC device can be explained in the following two ways as Figure 2 illustrates:

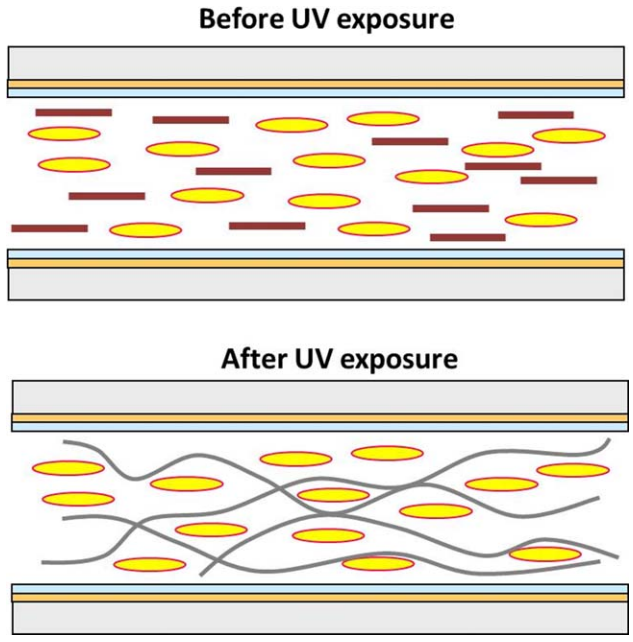

FIGURE 1 Fabrication procedure of a PNLC device. Upper: The mixture of LC host and photo-polymerizable monomer is filled into a homogeneous LC cell. Lower: Polymer network forms across the LC cell after UV exposure.

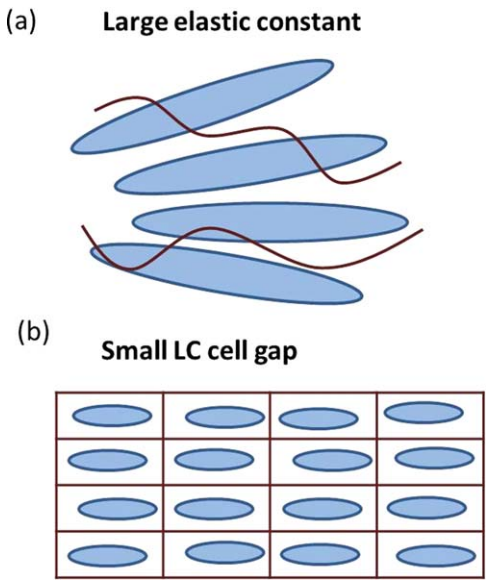

FIGURE 2 Two possible explanations for the fast response time of a PNLC device: a) large elastic constant, and b) small cell gap.

Macroscopic View: Large Elastic Constant

This model is convenient to use for device simulation since it treats a PNLC device with the same configuration as a nematic LC. According to ref. 24, the rotational viscosity γ_1 of a PNLC material remains the same as its nematic host after UV polymerization. Due to the strong anchoring of polymer network, the LC directors in a scattering-free PNLC require a larger electric field to deform, corresponding to a ~500–1000X larger splay elastic K_{11} value and faster response time.[23,24]

Microscopic View: Small Cell Gap

Microscopically speaking, a PNLC is completely different from nematic LC. In a PNLC device, LC molecules are partitioned into numerous nanoscale or micron-sized LC domains. The restoring force of the deformed LC directors no longer depends on the two LC substrates. Instead, the LC/polymer network interface plays the primary role in bringing LC molecules back during decay process. Therefore, the free relaxation time of PNLC can be written as:

$$\tau_0 = \frac{\gamma_1 D^2}{K_{11}\pi^2} \tag{3}$$

where D is the average domain size. This equation is useful to estimate the PNLC domainsize. The domain size of a typical scattering-free PNLC is in the order of ~200 nm.

Electro-Optical Properties

In the voltage-off state, PNLC device is highly transparent since LC molecules align well with the surface treatment. But after a voltage is applied, the LC molecules constrained by polymer network start to form multidomains, which scatter light if the domain sizes are comparable to the wavelength. As Figure 3 shows, the power-on scattering of PNLC

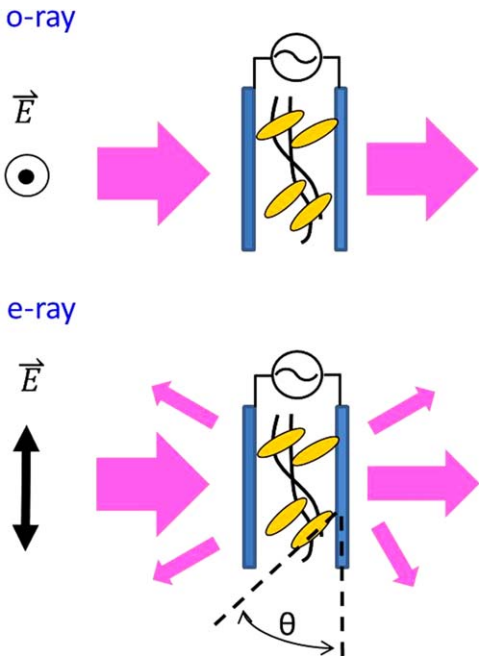

FIGURE 3 On-state scattering of PNLC is highly polarization dependent. The o-ray (polarization perpendicular to rubbing) has almost no scattering, but e-ray (polarization parallel to rubbing) has strong scattering.

device is highly polarization dependent. This is because LC molecules mainly rotate in the plane formed by the rubbing direction and the substrate normal direction. The effective refractive index for the extraordinary ray (polarization parallel to alignment direction) can be written as[31]

$$n_{e-eff} = \frac{n_o n_e}{\sqrt{n_o^2 \sin^2\theta + n_e^2 \cos^2\theta}} \tag{4}$$

where n_o and n_e are the ordinary and extraordinary refractive indices of the PNLC, and θ is the effective tilt angle as indicated in Figure 3. For an o-ray, the incident polarization is perpendicular to the LC alignment direction. Thus, n_o almost does not change with voltage; the power-on scattering of PNLC is mainly caused by the e-ray.

Although light scattering can be used for some display applications, it is very undesirable for SLM. To better understand the light scattering property of PNLC, a model based on Rayleigh–Gans–Debye approximation[26,32,33] has been proposed. To fulfill this approximation, the phase shift caused by the scattering domain should satisfy $D\delta n_{\text{eff}} << 2\pi\lambda_m$; here D is the average LC domain size, δn_{eff} is the refractive index difference at the grain boundary and λ_m is the wavelength in the medium, that is, $\lambda_m = \lambda_0/n$. According to this model, the scattering cross section can be written as:

$$\sigma_s \sim \left(\frac{\delta n_{eff}}{n}\right)^2 \frac{D^4}{\lambda_m^2} = (\delta n_{eff})^2 \frac{D^4}{\lambda_0^2} \tag{5}$$

We can obtain the extinction coefficient of PNLC by taking D^{-3} as the density of scattering center:

$$\alpha \sim \frac{\sigma_s}{D^3} = (\delta n_{eff})^2 \frac{D}{\lambda_0^2} \quad (6)$$

As the refractive index difference at the grain boundary is supposed to be proportional to theLC birefringence in PNLC, we can rewrite the extinction ratio as

$$\alpha = (\Delta n)^2 \frac{C}{\lambda_0^2} \quad (7)$$

where $C \sim DB^2$, $0<B<1$. If a voltage V_{max} leading to maximum scattering loss is applied to the PNLC cell, the refractive index difference $\delta n_{eff} \sim \Delta n$. Then, C becomes a domain size parameter proportional to D only. Without considering the reflection at interfaces, the transmittance of PNLC for a randomly polarized light at V_{max} can be written as:

$$T = \frac{1}{2}\exp\left(-C_e \frac{\Delta n^2}{\lambda_0^2} d\right) + \frac{1}{2}\exp\left(-C_o \frac{\Delta n^2}{\lambda_0^2} d\right) \quad (8)$$

where C_e and C_o represent the domain size parameters for e-ray and o-ray, respectively ($C_o << C_e$). For a low birefringence LC, it requires a thick LC layer to achieve a certain phase change, which may cause alignment issue and high operating voltage. Therefore, small domain size plays the key role in suppressing the scattering loss of a PNLC.

We used the experimental setup sketched in Figure 4 to evaluate the electro-optical properties of PNLC. For convenience, we used a laser as the probing light source. In transmissive mode, PNLC sample was sandwiched between two crossed polarizers with rubbing direction oriented at 45° with the polarization direction. In reflective mode, a mirror was placed behind the sample to double the optical path length. The angle between incident beam and reflected beam is below 5°. A computer controlled LabVIEW system was used to scan voltage to the PNLC sample and to record the detected light transmittance.

Monomer Effect

In order to shrink domain sizes and eliminate scattering for a PNLC device, several factors should be taken into consider-

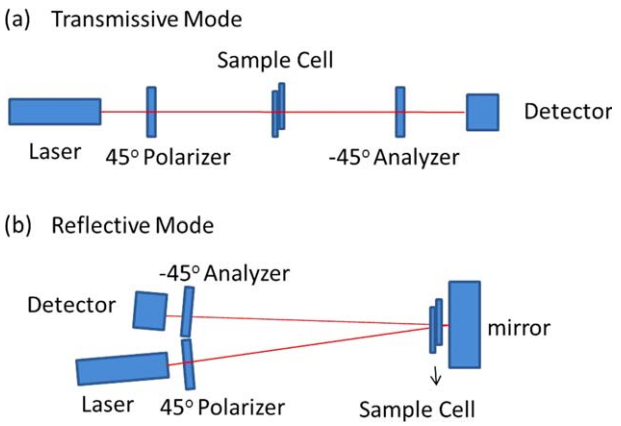

FIGURE 4 Experimental setup for characterizing the PNLC samples: (a) transmissive mode, and (b) reflective mode.

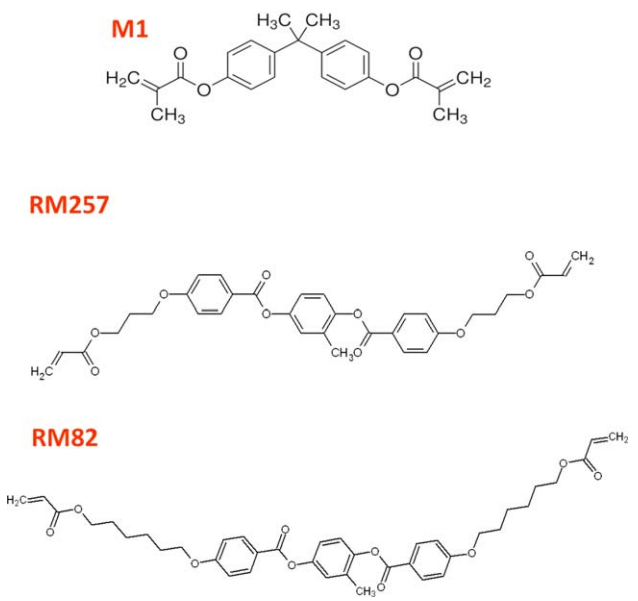

FIGURE 5 Examples of di-functional monomers used in PNLC.

ation, such as monomer, LC host, UV intensity, and photoinitiator concentration.[9,34] Here, we concentrate on the monomer and LC host effects.

Monomer plays an essential role in determining the PNLC domain sizes and operating voltage. A typical LC gel (scattering mode PNLC) contains 6–8 wt % di-functional monomer. Figure 5 lists some examples of difunctional monomers used in PNLC. As the monomer ratio increases, LC domain size decreases, leading to reduced scattering loss but increased operating voltage. By increasing the monomer ratio to 10%, a scattering-free PNLC (PNLC-A) was developed at $\lambda = 1.55$ μm.[23] The cell gap of PNLC-A is 12 μm. However, if we operate this PNLC at $\lambda = 1.06$ μm its scattering loss exceeds 20% because the scattering loss is strongly wavelength dependent according to eq 8. To suppress scattering, we increased the monomer ratio to 12% (PNLC-B).[24] Figure 6

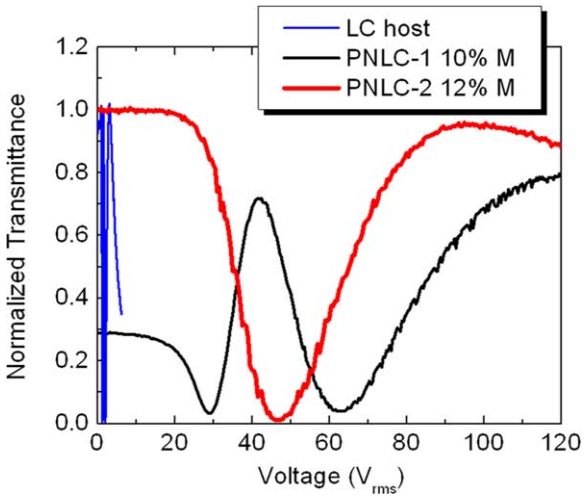

FIGURE 6 Measured VT curves of PNLC-A and PNLC-B at $\lambda = 1.06$ μm.

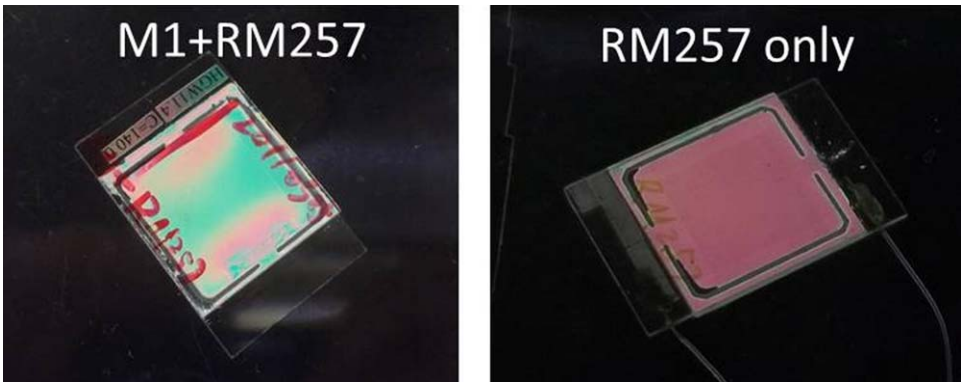

FIGURE 7 Photographs of two PNLCs containing different types of monomers.

depicts the measured voltage-dependent transmittance (VT) curves of PNLC-A and PNLC-B at 1.06 μm. Note that the peak transmittance of PNLC-B is comparable to that of a 12-μm nematic LC host cell, which means PNLC-B is free from scattering at $\lambda = 1.06$ μm. Due to the strong anchoring effect of polymer network and large elastic constant, both PNLCs exhibit submillisecond response time.

In PNLC-A and PNLC-B, we used a nonmesogenic monomer (M1, Fig. 5) to help reduce voltage. Although M1 helps lower the operating voltage, it disturbs the LC alignment. As a result, it causes nonuniform phase profile spatially, which is problematic for SLM. Figure 7 shows the photographs of two PNLC samples sandwiched between two crossed polarizers on a white light table. The left one containing both nonmesogenic monomer M1 and mesogenic monomer RM257 exhibits nonuniform color distribution due to the poor LC alignment while the right one (RM257 only) shows a uniform color. The problem is if we use 10–12% RM257 in a PNLC, the operating voltage would be quite high because M1 helps to create a large pretilt angle, which in turn weakens the anchoring force between polymer network and LC molecules. Therefore, new strategy is needed in order to use a minimal amount of polymer for reducing operation voltage while keeping stable networks and negligible scattering.

LC Host Effect

In a PNLC, nematic host occupies ~90% by weight, which plays the key role to determine the final performance. Recently, we found that the domain sizes also highly depend on the employed nematic LC host.[26] To verify this, we prepared a series of PNLC samples based on five different nematic hosts, whose physical properties are listed in Table 1. The power-on transmission spectra at V_{max} for these PNLCs were measured and results are shown in Figure 8(a). The following parameters are kept the same to all the samples: 6 wt % polymer (RM257), 0.5 wt % photoinitiator (Irgacure 819), curing temperature 22 °C, and cell gap 12 μm. All the spectra in Figure 8(a) are normalized to a 12-μm cell filled with BK7 matching liquid. Wavelength-dependent birefringence of these five LC host was measured and plotted in Figure 8(b). Through eq 8, we are able to extract the domain size parameters C_o and C_e from the transmission spectra of each PNLC sample. As $C_o << C_e$, we only plot C_e against $1/\gamma_1$ in Figure 9(a). It is found that the domain size of PNLCs is inversely proportional to the viscosity of the LC host.

According to eq 3, the PNLC response time is mainly determined by the average domain size. Thus, the free relaxation time should be inversely proportional to $\gamma_1 K_{11}$. This implies that a high viscosity LC host would result in a fast-response PNLC. This prediction is against our intuition, but is validated by our experimental results shown in Figure 9(b). A simple explanation is given as follows: A higher viscosity LC leads to slower diffusion rate during UV curing. Thus, the domain size is smaller, which in turn results in a faster response time.

Scattering-Free PNLC at 1.06 and 1.55 μm

The rotational viscosity follows the modified Arrhenius model: [35]

TABLE 1 Physical Properties of Five LC Hosts Used in PNLC 1-5 Measured at 22 °C

PNLC	LC Host	γ_1/K_{11} (ms/μm^2	γ_1 (Pa s)	K_{11} (pN)	$\Delta\varepsilon$ (1 kHz)	Δn at 1.06 μm	Δn at 633 nm
1	MLC14200 (Merck)	27.3	0.27	9.9	25	0.15	0.16
2	E44 (Merck)	27.3	0.33	12.1	16	0.22	0.24
3	BL038 (Merck)	40.7	0.56	13.8	16	0.23	0.25
4	HTG135200 (HCCH)	119.6	1.20	10.0	86	0.19	0.21
5	BP1 (HCCH)	153	1.52	9.9	50	0.15	0.15

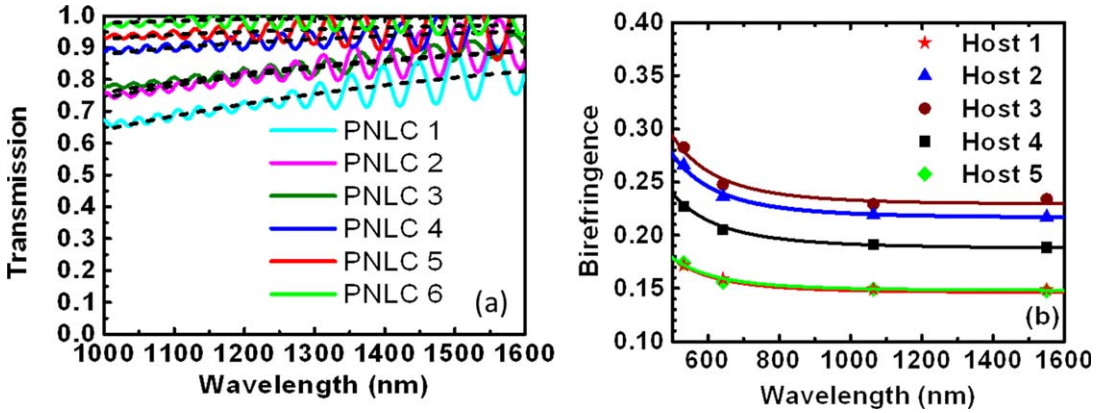

FIGURE 8 (a) Transmission spectra of PNLC 1–6 with V_{max} applied. Solid lines: experimental results; dashed lines: fitting results with eq 8. (b) Wavelength-dependent Δn of the five LC hosts.

$$\gamma_1 = b \cdot S \cdot \exp\left(E_a / k_B T\right) \tag{9}$$

where b is a proportionality constant, E_a is the activation energy due to the interaction potential resulting from microscopic friction between LC molecules, S is the order parameter, and K_B is the Boltzmann constant. From eq 9, the rotational viscosity of a nematic LC increases exponentially as the temperature decreases. With HTG 135200 as the LC host, we further shrink the PNLC domain size by reducing the curing temperature to 11 °C. The power-on transmission spectrum of this PNLC sample (PNLC-6) is included in Figure 8(a). Its scattering loss is <3% at $\lambda = 1.06$ μm and ~0% at $\lambda = 1.55$ μm. Please note that only 6 wt % polymer is employed in this sample.[26]

Figure 10 depicts the measured VT curve of PNLC 6 at $\lambda = 1.06$ μm. The 2π phase change voltage is 70 V, as indicated by the vertical dashed lines.

We also tested PNLC 6 at $\lambda = 1.55$ μm for both transmissive and reflective modes. Figure 11 shows the voltage-dependent phase shift. The required voltage for 2π phase change is $V_{2\pi} = 100$ V for transmissive mode and 53 V for reflective mode, respectively. Response time of this PNLC SLM is around 200 μs at 22 °C.

Scattering-Free PNLC at Visible Wavelengths

To extend the scattering-free feature to a visible wavelength, we have to reduce the PNLC domain size. A straightforward way is to increase the polymer concentration from 6 to 10 wt %.[27] To demonstrate the effectiveness of this approach, we prepared two PNLC samples based on two different LC hosts. Each sample contains 89.5 wt % LC host, 10 wt % RM257, and 0.5% photoinitiator (BAPO). The LC host for PNLC–vis is HTG-135200 (HCCH, China) and the LC host for PNLC-ref is MLC-14200 (Merck). Two homogeneous LC cells with $d = 5$ μm were used in this experiment. UV curing was conducted at 11 °C for both PNLC cells. A too-low curing temperature may cause fog on the substrate surfaces, which would truncate some UV light and cause nonuniform exposure.

Figure 12(a) shows the measured transmission spectra of PNLC–vis and PNLC-ref with unpolarized light. To present the worst scenario of light scattering, we applied a biased

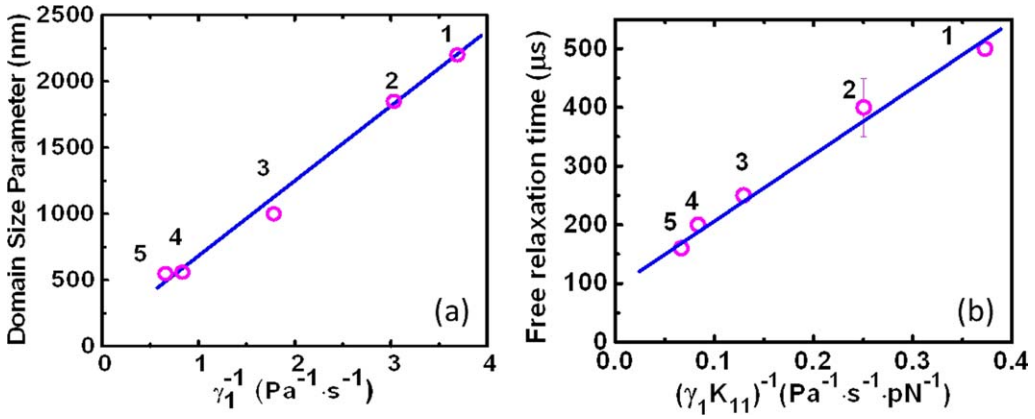

FIGURE 9 (a) Domain size parameter versus $1/\gamma_1$ for PNLC 1–5. (b) Free relaxation time versus $(\gamma_1 K_{11})^{-1}$ for PNLC 1-5. Straight lines are for visual guide.

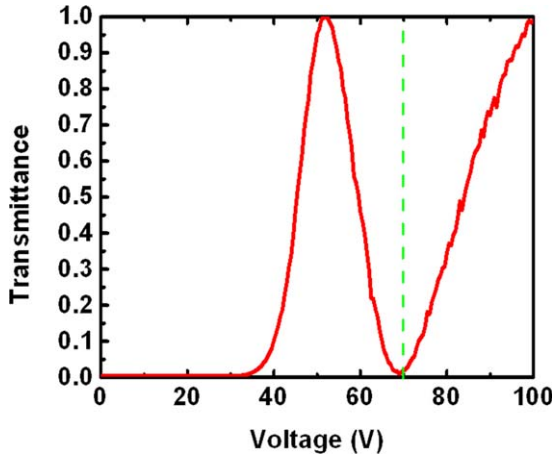

FIGURE 10 Measured VT curve of PNLC 6 at $\lambda = 1.06\ \mu$m. Vertical dashed lines indicate 2π phase shift.

voltage (V_{max}) to the PNLC cell where maximum scattering occurs. The sample was placed at 20 cm from the detector whose aperture is 9 mm, corresponding to $\sim 3^\circ$ collection angle. Such a small collection angle is to ensure that only transmitted light can reach the detector. If the PNLC cell has strong scattering, then the received transmittance at detector would be significantly reduced.

For benchmarking purpose, we also include the transmission spectrum of a control nematic LC cell (HTG-135200). The observed small oscillation in transmission originates from Fabry-Perot effect at the ITO/LC interfaces. From Figure 12(a), we find that the scattering loss of PNLC–vis in the power-on state is negligible at $\lambda = 633$ nm (and $\sim 3\%$ at $\lambda = 480$ nm) in reference to the nematic LC host. In contrast, the scattering loss of PNLC-ref in the visible region is much stronger (between 8 and 15%).

According to eq 8, small Δn, small domain size, and thinner cell gap help reduce scattering loss. However, to obtain 2π phase change, we need to maintain a certain $d\Delta n$ value. Knowing that MLC-14200 used in PNLC-ref has a lower birefringence than HTG-135200, we conclude that PNLC–vis should have much smaller domain sizes than PNLC-ref in order to explain why PNLC–vis has a negligible scattering loss.

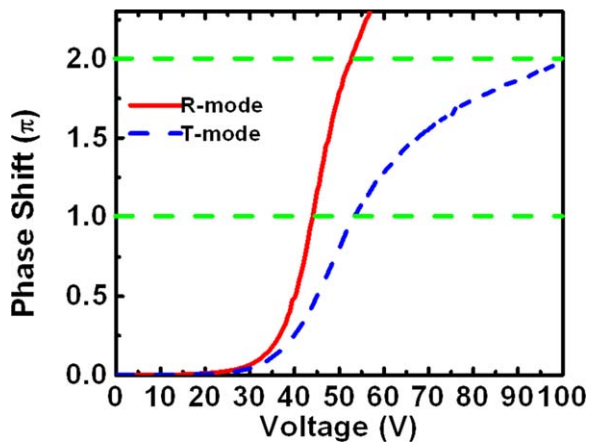

FIGURE 11 Measured voltage-dependent phase shift for PNLC 6 at $\lambda = 1.55\ \mu$m.

To compare the scattering characteristics visually, we used a polarized green laser ($\lambda = 514$ nm) to illuminate these two PNLCs at a power-on state. The polarization axis of the green laser beam is parallel to the rubbing direction of the LC cells. Figure 12(b) show the observed scattering phenomena for PNLC-ref and PNLC–vis, respectively. PNLC–vis is almost transparent to the laser beam while PNLC-ref scatters light heavily. This scattering-free PNLC opens a new gateway for photonic devices in the visible region.

Figure 13 depicts the VT curves of PNLC–vis at two visible wavelengths: $\lambda = 633$ and 488 nm and at room temperature (22 °C). Also included for comparison is a nematic LC cell (green curve). The transmission peak of PNLC–vis at red and blue wavelengths is about the same as that of nematic cell, indicating the scattering loss is indeed negligible.

From Figure 13, we can calculate the voltage-dependent phase change of PNLC–vis. Results are shown in Figure 14 for $\lambda = 633$ nm. Here, the blue curve is for transmissive mode and red is for reflective mode.

Figure 15 depicts the measured temperature-dependent response time of PNLC–vis at reflective mode. At 22 °C, the

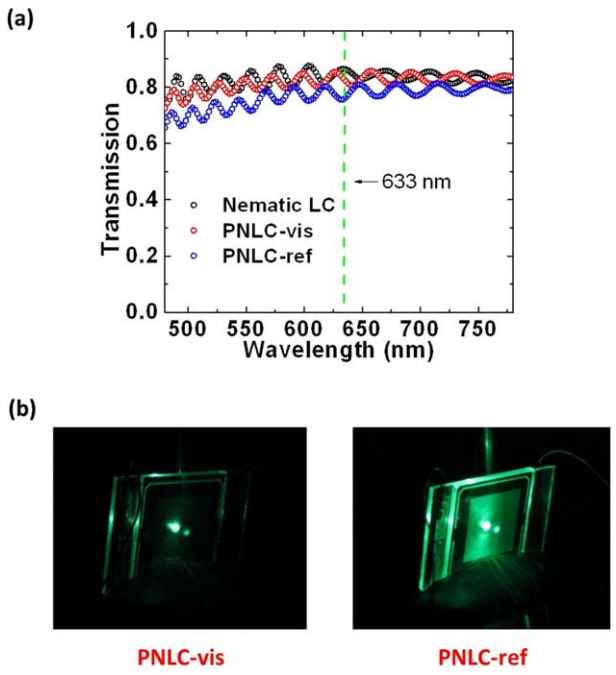

FIGURE 12 (a) Measured transmission spectra of PNLC–vis (red symbols) and PNLC-ref (blue symbols) at the maximum scattering states (with V_{max} applied). For comparison, the transmission spectrum of a nematic LC cell is included (black symbols). (b) Light scattering of PNLC–vis and PNLC-ref illuminated with a green laser ($\lambda = 514$ nm).

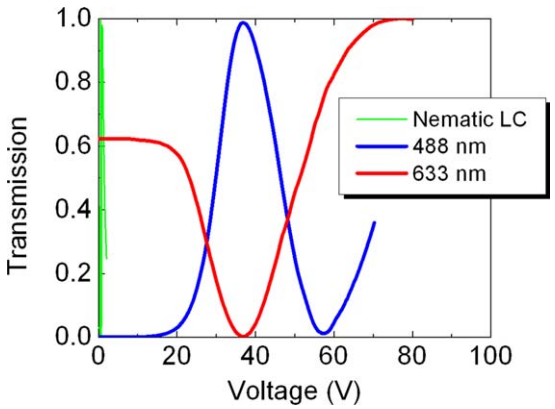

FIGURE 13 Measured VT curves of scattering-free PNLC–vis cell at λ = 633 nm and 488 nm and RT = 22 °C. The green curve is for the nematic cell. Cell gap d = 5 μm, and pretilt angle~3°.

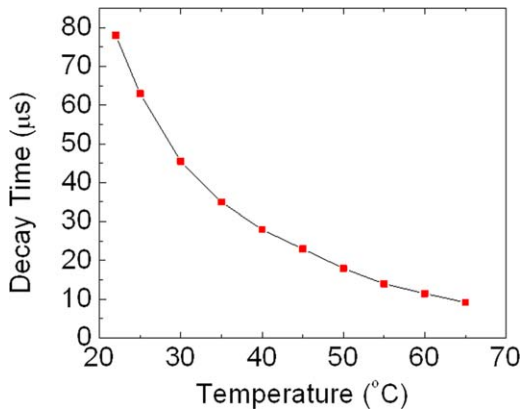

FIGURE 15 Measured temperature-dependent decay time of PNLC–vis for a 2π phase change at reflective mode. λ = 633 nm, d = 5 μm, and pretilt angle~3°.

decay time (90–10% phase change) is 78 μs. Such a fast response time results from submicron domain sizes. As the temperature increases, the decay time decreases accordingly. At 65 °C, the decay time is 9.2 μs due to the dramatically decreased viscosity.

DISCUSSION

Our current PNLC–vis requires $V_{2\pi}$~49 V to obtain 2π phase change in reflective mode at λ = 633 nm. However, the commonly used reflective SLM, liquid-crystal-on-silicon (LCOS),[36–39] has a maximum voltage of 24 V. To reduce operating voltage, a simple approach is to use a high $\Delta\varepsilon$ LC host. Nematic LC host with $\Delta\varepsilon$ greater than 100 has already been adopted in polymer-stabilized blue phase LC devices.[40–42] A major concern of this approach is that the dielectric relaxation frequency of such a huge $\Delta\varepsilon$ LC is relatively low (~1 kHz).[18,43]

In addition to high $\Delta\varepsilon$, anchoring energy, pretilt angle, and Δn also play important roles affecting the operation voltage.[44,45] From Figure 14, the on-state voltage consists of two parts: threshold voltage (V_{th}) and swing voltage ($\Delta V = V_{2\pi} - V_{th}$). The threshold voltage is governed by the pretilt angle and square root of $K_{11}/\Delta\varepsilon$. On the other hand, the swing voltage is mainly determined by Δn and λ.

Figure 16 shows the simulated birefringence effect on the operation voltage of a reflective PNLC at λ = 633 nm. As Δn increases, $V_{2\pi}$ gradually decreases. If Δn = 0.3, then $V_{2\pi}$ ~ 35 V and ΔV < 20 V, assuming $\Delta\varepsilon$ remains the same as that shown in Figure 14.

Figure 17 shows the simulated pretilt angle effect on the phase change and operating voltage of a PNLC at λ = 633 nm. As pretilt angle increases from 5° to 45°, the threshold behavior is gradually smeared. However, the total phase change gets smaller because of the decreased effective birefringence. Therefore, there exists an optimal pretilt angle. To

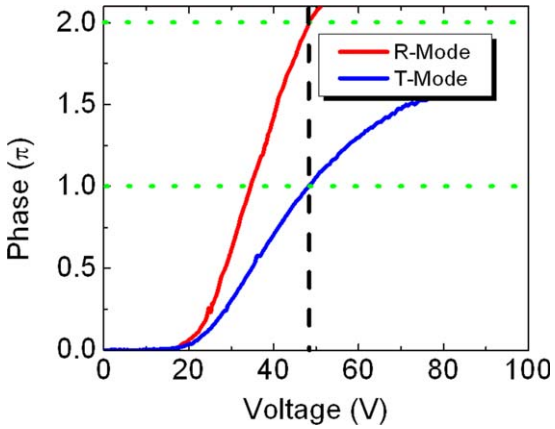

FIGURE 14 Measured voltage-dependent phase change of PNLC–vis at λ = 633 nm and RT for T-mode (blue) and R-mode (red) operations. Cell gap d = 5 μm and pretilt angle~3°.

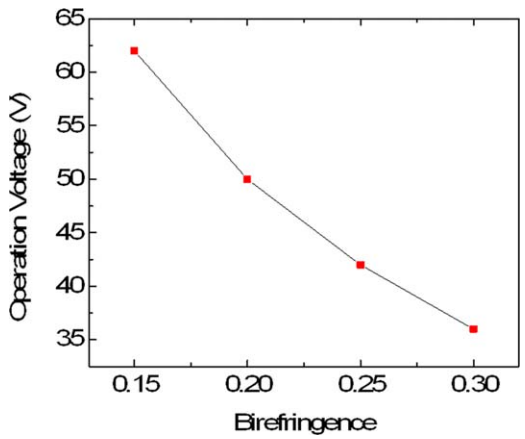

FIGURE 16 Birefringence effects on $V_{2\pi}$ of a reflective PNLC at λ = 633 nm. Here, the pretilt angle is assumed to be 3°.

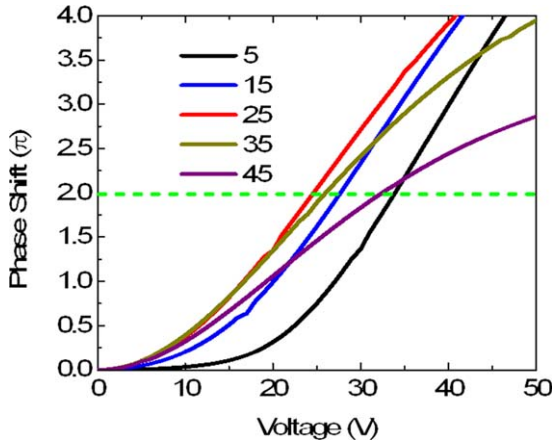

FIGURE 17 Simulated pretilt angle effect on the phase change of PNLCs in reflective mode at $\lambda = 633$ nm. Cell gap $d = 5$ μm, $\Delta\varepsilon = 86$, and $\Delta n = 0.3$.

obtain 2π phase change for LCOS, the lowest on-state voltage can achieve 24 V when the pretilt angle is $\sim 25^\circ$ (red line).

Next, we fix the phase change at 2π for a reflective mode and then calculate which pretilt angle would lead to the lowest on-state voltage. Results are plotted in Figure 18. For 2π phase change, the lowest V_{on} can achieve 24 V with pretilt angle $\sim 25^\circ$. The results are basically consistent with those shown in Figure 17.

CONCLUSIONS

We have reviewed recent progress on the development of submillisecond-response and scattering-free PNLC SLMs from $\lambda = 1.55$, 1.06 μm, to ~ 0.5 μm. The 2π operation voltage of our current PNLC is ~ 49 V in reflective mode at $\lambda = 633$ nm. By considering the birefringence and pretilt angle effects, a LCOS with $V_{2\pi}$ below 24 V can be achieved according to our device simulation.

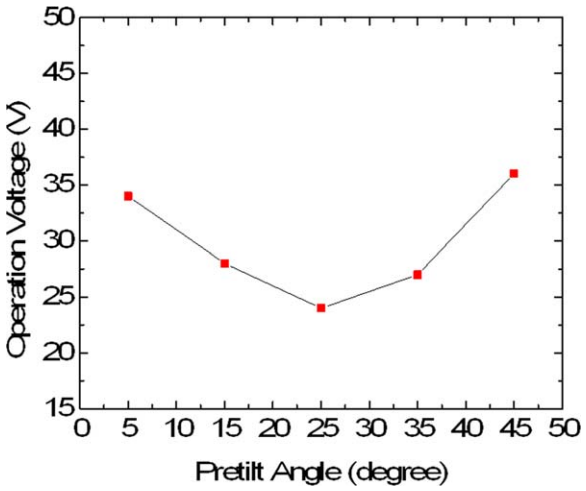

FIGURE 18 Simulated pretilt angle effect on the operating voltage of PNLC cells at $\lambda = 633$ nm for 2π phase change in reflective mode. Cell gap $d = 5$ μm, $\Delta\varepsilon = 86$, and $\Delta n = 0.3$.

ACKNOWLEDGMENTS

This work is supported by AFOSR under contract No. FA95550-09-1-0170.

REFERENCES AND NOTES

1 U. Efron, Spatial Light Modulator Technology: Materials, Devices, and Applications; Marcel Dekker, New York, **1995**.

2 M. Reicherter, S. Zwick, T. Haist, C. Kohler, H. Tiziani, W. Osten, *Appl. Opt.* **2006**, *45*, 888-896.

3 C. Kohler, X. Schwab, W. Osten, *Appl. Opt.* **2006**, *45*, 960-967.

4 P. Clemente, V. Durán, E. Tajahuerce, P. Andrés, V. Climent, Lancis, *J. Opt. Lett.* **2013**, *38*, 2524-2527.

5 Y.-P. Huang, C.-W. Chen, Y.-C. Huang, *J. Display Technol.* **2012**, *8*, 650-655.

6 P. F. McManamon, T. A. Dorschner, D. L. Corkum, L. J. Friedman, D. S. Hobbs, M. Holz, S. Liberman, H. Q. Nguyen, D. P. Resler, R. C. Sharp, E. A. Watson, *Proc. IEEE* **1996**, *84*, 268-298.

7 G. D. Love, *Appl. Opt.* **1997**, *36*, 1517-1520.

8 L. Hu, L. Xuan, Y. Liu, Z. Cao, D. Li, Q. Mu, *Opt. Express* **2004**, *12*, 6403-6409.

9 T. J. Bunning, L. V. Natarajan, V. P. Tondiglia, R. L. Sutherland, *Annu. Rev. Mater. Sci.* **2000**, *30*, 83-115.

10 S. T. Wu, D. K. Yang, Fundamentals of Liquid Crystal Devices; Wiley, Hoboken, NJ, **2006**.

11 S.-T. Wu, C.-S. Wu, *Appl. Phys. Lett.* **1988**, *53*, 1794-1796.

12 S.-T. Wu, *Phys. Rev. A* **1986**, *33*, 1270-1274.

13 W. J. De Jeu, C. J. Gerritsma, P. Van Zanten, W. J. A. Goossens, *Phys. Lett. A* **1972**, *39*, 355-356.

14 J. Sun, H. Xianyu, S. Gauza, S.-T. Wu, *Liq. Cryst.* **2009**, *36*, 1401-1408.

15 S. A. Serati, X. Xia, O. Mughal, A. Linnenberger, *Proc. SPIE* **2003**, *5106*, 138-145.

16 M. Schadt, *Mol. Cryst. Liq. Cryst.* **1981**, *66*, 319-336.

17 H. Kikuchi, M. Yokota, Y. Hisakado, H. Yang, T. Kajiyama, *Nat. Mater.* **2002**, *1*, 64-68.

18 Y. Li, Y. Chen, J. Sun, S.-T. Wu, S.-H. Liu, P.-J. Hsieh, K.-L. Cheng, J.-W. Shiu, *Appl. Phys. Lett.* **2011**, *99*, 181126.

19 Y. Chen, J. Yan, J. Sun, S.-T. Wu, X. Liang, S.-H. Liu, P.-J. Hsieh, K.-L. Cheng, J.-W. Shiu, *Appl. Phys. Lett.* **2011**, *99*, 201105.

20 J. Fünfschilling, M. Schadt, *Jpn. J. Appl. Phys.* **1991**, *30*, 741-746.

21 L. Beresnev, V. Chigrinov, D. Dergachev, E. Poshidaev, J. Fünfschilling, M. Schadt, *Liq. Cryst.* **1989**, *5*, 1171-1177.

22 R. A. M. Hikmet, *J. Appl. Phys.* **1990**, *68*, 4406-4412.

23 Y.-H. Fan, Y.-H. Lin, H. Ren, S. Gauza, S.-T. Wu, *Appl. Phys. Lett.* **2004**, *84*, 1233-1235.

24 J. Sun, H. Xianyu, Y. Chen, S.-T. Wu, *Appl. Phys. Lett.* **2011**, *99*, 021106.

25 J. Sun, R. A. Ramsey, C. Yuan, S.-T. Wu, *J. Disp. Technol.* **2012**, *8*, 87-90.

26 J. Sun, Y. Chen, S.-T. Wu, *Opt. Express* **2012**, *20*, 20124-20129.

27 J. Sun, S. Xu, H. Ren, S.-T. Wu, *Appl. Phys. Lett.* **2013**, *102*, 161106.

28 J. Heo, W.-D. Jang, O. Kwon, J. Ryu, J. Tan, H. Kim, Y. Jun, *Macromol. Res.* **2008**, *16*, 586-589.

29 H. Eimura, M. Yoshio, Y. Shoji, K. Hanabusa, T. Kato, *Polym. J.* **2012**, *44*, 594-599.

30 S. Bi, H. Peng, S. Long, M. Ni, Y. Liao, Y. Yang, Z. Xue, X. Xie, *Soft Matter* **2013**, *9*, 7718-7725.

31 S. T. Wu, *Appl. Opt.* **1989**, *28*, 48–52.

32 Y. K. Fung, A. Borstnik, S. Zumer, D. K. Yang, J. W. Doane, *Phys. Rev. E* **1997**, *55*, 1637-1645.

33 R. Apetz, M. P. B. van Bruggen, *J. Am. Ceram. Soc.* **2003**, *86*, 480-486.

34 I. Dierking, *Adv. Mater.* **2000**, *12*, 167-181.

35 S.-T. Wu, C.-S. Wu, *Phys. Rev. A* **1990**, *42*, 2219-2227.

36 K. M. Johnson, D. J. McKnight, I. Underwood, *IEEE J. Quant. Elect.* **1993**, *29*, 699-714.

37 X. Wang, J. Pouch, J. E. Anderson, P. J. Bos, F. Miranda, B. Wang, *Opt. Eng.* **2004**, *43*, 2769-2774.

38 E. J. Fernández, P. M. Prieto, P. Artal, *Opt. Express* **2009**, *17*, 11013-11025.

39 A. Ö. Yöntem, L. Onural, *J. Opt. Soc. Am. A* **2011**, *28*, 2359-2375.

40 L. Rao, J. Yan, S.-T. Wu, S.-I. Yamamoto, Y. Haseba, *Appl. Phys. Lett.* **2011**, *98*, 081109.

41 M. Wittek, N. Tanaka, D. Wilkes, M. Bremer, D. Pauluth, J. Canisius, A. Yeh, R. Yan, K. Skjonnemand, M. K. Memmer, *SID Int. Symp. Dig. Tech. Papers* **2012**, *43*, 25–28.

42 Y. Chen, D. Xu, S.-T. Wu, S.-I. Yamamoto, Y. Haseba, *Appl. Phys. Lett.* **2013**, *102*, 141116.

43 Y. Chen, J. Yan, M. Schadt, S. H. Liu, K. L. Cheng, J. W. Shiu, S. T. Wu, *J. Display Technol.* **2013**, *9*, 592-597.

44 X. Nie, H. Xianyu, R. Lu, T. X. Wu, S. T. Wu, *J. Appl. Phys.* **2007**, *101*, 103110.

45 X. Nie, H. Xianyu, R. Lu, T. X. Wu, S. T. Wu, *J. Display Technol.* **2007**, *3*, 280-283.